Computer Methods and Programs in Biomedicine (2005) **79**, 1–17

ELSEVIER

Computer Methods and Programs in Biomedicine

www.intl.elsevierhealth.com/journals/cmpb

Automatic extraction of brain surface and mid-sagittal plane from PET images applying deformable models

Jouni Mykkänen[a,*], Jussi Tohka[b], Jouni Luoma[c], Ulla Ruotsalainen[b]

[a] *Department of Computer Sciences, University of Tampere, Kanslerinrinne 1, Pinni B1039, FIN-33014, Finland*
[b] *Institute of Signal Processing, Tampere University of Technology, Finland*
[c] *Ionific Ltd., Tampere, Finland*

Received 27 February 2004; received in revised form 8 March 2005; accepted 14 March 2005

KEYWORDS
Brain surface extraction;
FDG brain images;
Raclopride brain images;
Segmentation;
Deformable surface

Summary In this study, we propose and evaluate new methods for automatic extraction of the brain surface and the mid-sagittal plane from functional positron emission tomography (PET) images. Designing methods for these segmentation tasks is challenging because the spatial distribution of intensity values in a PET image depends on the applied radiopharmaceutical and the contrast to noise ratio in a PET image is typically low. We extracted the brain surface with a deformable model which is based on a global optimization algorithm. The global optimization allows reliable automation of the extraction task. Based on the extracted brain surface, the mid-sagittal plane was determined. The method was tested with the image of the Hoffman brain phantom (FDG) and the images from the brain studies with the FDG (17 images) and the ^{11}C-Raclopride tracers (4 images). In addition to the brain surfaces, we applied the deformable model for extraction of the coarse cortical structure based on the tracer uptake from FDG-PET brain images. The proposed segmentation methods provide a promising direction for automatic processing and analysis of PET brain images.

1. Introduction

Positron emission tomography (PET) can be used to study biochemical processes involved in living organs like the brain. Identification of the brain volume from a PET image is a basis for many applications in the functional image analysis. It allows to locate and study sub-volumes of the brain, for example, the cortical hemispheres. Segmentation

* Corresponding author. Tel.: +358 3 35516193; fax: +358 3 35516070.
E-mail addresses: jouni.mykkanen@cs.uta.fi (J. Mykkänen), jussi.tohka@cs.tut.fi (J. Tohka), jouni.luoma@ionific.com (J. Luoma), ulla.ruotsalainen@tut.fi (U. Ruotsalainen).

0169-2607/$ — see front matter.
doi:10.1016/j.cmpb.2005.03.003

of, or extraction of volumes of interest (VOI) from the PET images is important for regional quantification. The entirely manual extraction of VOIs is not practical for a large set of PET images because it is time consuming work and the VOIs delineated by different human analyzers can differ. Intensity-based segmentation methods like thresholding and clustering could be applied, but they require user-interaction and manual editing of the extracted VOIs. A standard procedure to delineate structures according to their surfaces from the PET brain images is to segment the corresponding anatomical magnetic resonance (MR) images and then to superimpose the found anatomical surfaces on the PET images. This requires an accurate coregistration between the PET and MR images which is often performed manually, see, e.g. [1]. Automatic image registration is not a trivial task due to initial incongruity of structure and function, and fundamental differences between PET images acquired with different radiopharmaceuticals. For more information about the image registration methods available for nuclear medicine we refer to the survey [2].

The biochemical process described by a PET image is defined by the applied radiopharmaceutical from which also the spatial distribution of intensity values in the image depends on. Furthermore, PET images are typically noisy. Therefore, designing automatic and generally applicable structure extraction methods is a challenging task. By a structure in a PET image we mean a volume in the image, which has distinguishable (positive) uptake of the radiopharmaceutical from its surroundings. We have addressed brain structure extraction within PET in earlier studies. The thresholding method for extracting structures interactively from the PET brain images was studied in [3]. A sagittal slice was interactively determined from the PET image to separate the image into two parts roughly corresponding the two hemispheres to be able to set thresholds for both parts separately. This simple method was applied to extract the structures corresponding to the left and the right striatum from the D_2 receptor tracer FDOPA (6-[^{18}F]-L-dopa) PET images. We have examined two-dimensional (2D) generalized snakes (g-snakes) [4] for extraction of the structure corresponding the cortex from selected planes of the FDG (2-[^{18}F]-fluoro-2-deoxy-D-glucose) PET brain images in [5]. However, while the results obtained with the g-snakes were encouraging, it was impossible to use the 2D method to process the three-dimensional (3D) image volumes automatically. Besides, we applied also information from the corresponding MR image for the segmentation and therefore use of this method for registration purposes would be problematic.

In this study, we propose and evaluate an automatic method for extraction of the brain surface from the FDG and Raclopride PET images acquired from healthy volunteers. The extraction is based on a new 3D deformable surface model developed in our research group [6]. An important property of the deformable model is its low sensitivity to its initialization achieved by global minimization of its energy. This allows generation of initializations completely without user guidance, which is important if a large set of images is to be processed. Based on the found brain surface, we continue by determining the mid-sagittal plane. We also consider extraction of a structure corresponding cortex from the FDG-PET images using the deformable model. The proposed method is relying on data only from PET images themselves and therefore delineated surfaces could be used for registration purposes. Some surface extraction results with the FDG-PET images have been presented previously in [7,8]. Preliminary experiments for extracting the mid-sagittal plane from the FDG-PET brain images have been presented in [9].

2. Background

2.1. PET images

Positron emission tomography provides a unique method to investigate physiological processes in the brain. The distribution of the intensity values in a PET image depends on the applied radiopharmaceutical. For example, the receptor type tracers, like Raclopride, have uptake mainly in the structures having the highest densities of the corresponding receptors, whereas the tracers describing metabolic functions like FDG, which is the tracer for glucose consumption, have uptake all over the brain area, and the highest uptake in the cortical region. A functional structure in a PET image can be defined as a volume having distinguishable different, normally higher intensity values than its surroundings. Low contrast to noise ratio in the PET images causes problems for those segmentation methods, which are based only on intensity values. Fig. 1 presents the intensity histograms of one of the FDG-PET and one of the Raclopride PET brain images collected for this study. From the histograms it is clear that the voxels in a PET brain image cannot be classified similarly as the voxels in anatomical MR images because there is no grouping of intensity values around some structure bound mean value. Thus, the use of intensity-based segmentation methods needs interaction in the definition of

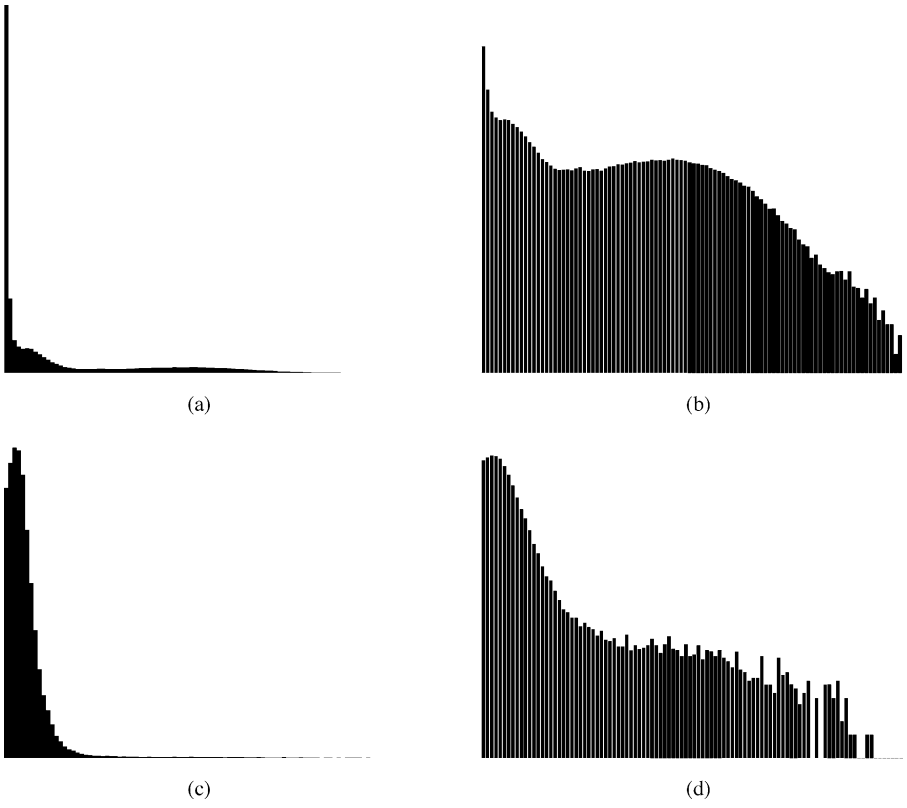

Fig. 1 The histogram of an image from the FDG-PET study with (a) linear scaling and (b) logarithmic scaling and from the Raclopride study with (c) linear scaling and (d) logarithmic scaling. Intensity values equaling zero are not included in the histograms.

meaningful threshold values for extraction of VOI. For automatic extraction, a more advanced segmentation method is required which should be resistant to noise and it should also be able to deal with the whole functional structure. This can be achieved if also a priori information of the approximate position and size of the object to be searched for can be included in the segmentation process.

The quality of PET images depends on the applied image reconstruction method. The positron emission data acquisition is subject to a substantial amount of statistical noise, originating from the statistical nature of the decay of the positron emitting isotope used for labeling the tracer molecule. The conventional filtered back-projection (FBP) image reconstruction produces images with noise and reconstruction artifacts. The iterative image reconstruction methods, especially those including noise regularisation in the reconstruction process produce better image quality. We have introduced iterative median root prior (MRP) reconstruction method, which has shown to produce outstanding noise reduction properties without blurring the edges in the images [10]. It is obvious that improved image quality, especially sharp edges and controlling of the noise content, helps the segmentation of PET images.

2.2. Deformable models

Deformable surface models are advanced methods for image segmentation and surface extraction. They use prior information about the geometry of objects of interest in addition to the image data. Therefore, they are not as sensitive to imperfections in the image data as those segmentation methods, which rely solely on the image data. As a consequence, deformable models have found various applications within analysis of medical images [11].

A deformable model consists of a geometric representation of a surface and evolution rules that control the adaptation of the surface shape according to the image data. The shape adaptation is often formulated as an energy minimization problem. The energy function of a deformable surface model consists of an external energy term derived from the image data and an internal energy term, which depends only on the properties of surfaces themselves. A common drawback of deformable models

is that the formulated energy minimization problem is difficult to solve due to numerous local minima. This easily leads to problems with the initialization of deformable models. In other words, the initial surface has to be in a close vicinity of the target surface in order for a standard deformable model to converge to a correct solution. There exist several advanced methods that have been proposed to solve the initialization sensitivity problem, but reviewing these would be outside of the topic in this study.

2.2.1. Deformable models for MR brain images

Deformable models have been used extensively for analysis of the 3D MR brain images. We review briefly a few applications of them and point out how processing of PET images differs from these applications.

The extraction of cerebral cortex from MR images is a difficult task because the complex shape of the cortex is problematic to capture properly. MacDonald et al. [12] considered automatic extraction of the inner and outer surfaces of the cortical gray matter from the MR images. They first classified voxels in a MR image according to their tissue type. Thereafter, a deformable surface-based on simple coarse-to-fine optimization was used to locate boundary between the gray and white matter, the inner surface of the cerebral cortex. Starting from the inner surface of cortex and applying proximity constraints, the outer surface of the cortex was extracted. The method depends on voxel classification and therefore it is not directly applicable for PET images.

Xu et al. [13] proposed to use a generalized gradient vector flow (GGVF)-based deformable model [14] to obtain a representation of the central layer of the cerebral cortex. They also first classified images according to the tissue types and then generated initializations for deformable surfaces based on voxel classifications. The initialization stage required some user interaction. The GGVF deformable models do not necessarily require voxel classification prior to their application.

Shen et al. [15] extracted ventricles and nuclei from the MR brain images using a deformable surface model. They relied on edge-detection instead of voxel classification in the formulation of the external energy for their deformable model. However, they applied a rather complex shape modeling scheme requiring hand-crafted example surfaces.

2.2.2. Deformable models for PET images

Deformable surface models are attractive methods for analysis of the anatomical MR images. Due to differences between PET images and MR images that were explained in Section 2.1, the direct application of deformable models designed for MR images is not necessarily plausible for analysing PET image data. However, deformable models have been considered also within PET and single photon emission computed tomography (SPECT) although not as extensively as within MR imaging. Also, within PET or SPECT, most of the applications of deformable models seem to focus on cardiac images. Bardinet et al. [16] used deformable models for extraction of the left ventricle of the heart from the cardiac SPECT images. The deformable model combined superquadrics with few degrees of freedom to free form deformations in order to properly segment noisy images. The method relies on thresholding of images and the selection of the threshold value appears to require user-guidance. Noumeir and El-Daccache [17] applied a 3D generalization [18] of the snakes algorithm [19] for attenuation correction with the cardiac SPECT images. However, based on the short description of the algorithm it is hard to deduct the level of automation of their method. The deformable motion algorithm was presented in [20], to compensate for patient motion in gated PET cardiac images. However, as this problem is quite different from ours, we do not consider it further here. In [21], the level-set based deformable models [22] were applied to segmentation of the four-dimensional (4D) (3D and time) gated myocardial SPECT images. In our applications, it is favorable to constrain topologies of the extracted surfaces, and therefore the level-set techniques are of limited interest for us.

Tohka [23] has studied brain surface extraction from PET images using different deformable models. A preliminary version of the deformable model applied in this study was featured in the study. Tohka concluded that the problem seems to be hard if automatic use of deformable models is desired. However, two deformable models, the one considered in this study and the GGVF-based model [14] yielded good extraction results. As stated in [23], the results of such a study are open to many interpretations and drawing too strict conclusions about superiority of one method over the others for the task should be avoided.

2.3. Extraction of mid-sagittal plane from PET brain images

Differences in brain functions between the two hemispheres are interesting in neurological research. To study these differences, the hemispheres must be separated in a brain image. This can be

done by identifying the mid-sagittal plane of the brain. The mid-sagittal plane can be defined as the one plane about which the reflective symmetry of the brain is maximized in the image. Several measures have been used as the symmetry criterion within PET. Ardekani et al. [24] considered the cross-correlation of the intensity values between the hemispheres as the symmetry criterion. This criterion is obviously sensitive to asymmetries and anisotropy of intensity values between the hemispheres. Prima et al. [25] used the block-matching and robust regression techniques to find the mid-sagittal plane even when there exist a normal or abnormal asymmetry in the brain.

Also, symmetry criteria that are not directly related to intensity values can be considered. Liu et al. [26] considered the symmetry of edge-images rather than symmetry of the original intensity images. They applied their method only for anatomical MR or CT images. In this study, we extend their method for functional PET images. However, it could be expected that edge-images would not have a quality good enough for reliable determination of the mid-sagittal plane. Therefore, we base our mid-sagittal plane extraction algorithm to the PET brain surfaces that were extracted by the deformable surface model.

3. Deformable surface model

Surfaces are extracted from volumetric images by minimizing the energy function of the deformable model. Surfaces are approximated by simplex meshes [27]. A set of discrete points $\boldsymbol{W} = \{\boldsymbol{w}_1, \boldsymbol{w}_2, \ldots, \boldsymbol{w}_n\}$, called mexels ($\in \mathbb{R}^3$), and adjacency relations between mexels define a simplex mesh. Adjacency relations are known and constant, hence the symbol $\boldsymbol{W}$ is used for a simplex mesh.

3.1. Energy model

The total energy of the surface mesh $\boldsymbol{W}$ is defined as

$$E(\boldsymbol{W}) = \lambda E_{\text{int}}(\boldsymbol{W}) + (1-\lambda)E_{\text{ext}}(\boldsymbol{W}) = \frac{1}{n}\sum_{i=1}^{n}(\lambda E_{\text{int}}(\boldsymbol{w}_i) + (1-\lambda)E_{\text{ext}}(\boldsymbol{w}_i)). \quad (1)$$

The regularisation parameter λ is in range $[0, 1]$. The external energy E_{ext} couples $\boldsymbol{W}$ to the salient image features. The internal energy E_{int} regularizes the shape of the surface.

3.1.1. Internal energy

The mexel-wise internal energy is defined as

$$E_{\text{int}}(\boldsymbol{w}_i) = \frac{\|\boldsymbol{w}_i - \alpha\sum_{j=1}^{3}\boldsymbol{w}_{i_j}\|^2}{A(\boldsymbol{W})}, \quad (2)$$

where $\boldsymbol{w}_{i_j}$ are the neighbouring mexels of $\boldsymbol{w}_i$ in the mesh, $A(\boldsymbol{W})$ the average area of the faces of the mesh and α is the shape parameter. The shape parameter defines the favored shape for the internal energy. For the thin-plate shape model,

$$\alpha = \frac{1}{3}. \quad (3)$$

The thin-plate shape model states that each mexel should be positioned as near as possible to the centre of mass of its neighbouring mexels. For the sphere shape model derived in [6]

$$\alpha = \left(3\cos\left(2\arctan\frac{2(\sqrt{\pi\sqrt{3}})}{3(\sqrt{n})}\right)\right)^{-1}, \quad (4)$$

where n is the number of mexels in the mesh. The sphere shape model assumes that the optimal shape for the mesh is the sphere. The sphere shape model is more complicated, but applying it has often lead to better results than applying the simpler thin-plate shape model in our experiments. The reasons behind this are not trivial and are discussed in [6].

3.1.2. External energy

The precise form of the external energy function depends on the applied tracer because different image-features characterize surfaces of interest with different tracers. Therefore, for notational simplicity, we define the external energy with the help of energy images. An energy image is generated from the image to be processed in such a way that intensity values in the energy image describe saliency of voxels for the application and the tracer. The external energy at the position $\boldsymbol{w}$ is

$$E_{\text{ext}}(\boldsymbol{w}) = 1 - B(\boldsymbol{w}), \quad (5)$$

where B is the energy image. The energy image is normalized to have intensity values from 0 to 1. The generation of the energy images based on the original images is explained in Section 4.1.

3.2. Energy minimization

The energy function (1) is likely to have multiple local minima. Therefore, extracted surfaces obtainable by a local energy minimization would depend highly on the provided initializations. In our application, this could cause substantial problems in automating the surface extraction. We proposed a

global dual surface minimization (DSM) algorithm for the deformable mesh optimization in [6]. The algorithm is global in the sense that it can overcome local minima and hence it reduces the sensitivity of the deformable mesh to its initialization considerably. The algorithm is based on the iterative optimization of two surface meshes, which approach the surface of interest from different directions. We name the energy based deformable model (DM) with the DSM algorithm as the DM-DSM method.

3.2.1. Standard DSM algorithm

The DSM algorithm begins with two meshes: the outer mesh and the inner mesh. These are created from a given initial mesh preserving its properties, except the size. Their sizes are set in such a way that the surface of the searched structure lies in the space between them. This is the search volume for the minimization process.

The search is based on the iterative minimization of the energies of the outer and inner surfaces. The energies for the both surfaces are calculated from Eq. (1). During each iteration, the energy of the mesh is minimized using a greedy method adapted from [28]. It is used in such a way, that the outer surface shrinks and the inner surface grows. After each iteration, the DSM algorithm compares the energies of the outer and inner surfaces and continues minimization from the surface having higher energy. If the surface having higher energy gets stuck in a local energy minimum, the energy of the current surface position is forced to increase until the surface moves again. The DSM algorithm is stopped when the volume inside of the inner surface exceeds the volume inside the outer surface. The algorithm selects the surface having the lower energy as the result.

3.2.2. DSM-OS algorithm

Sometimes, for example, when extracting brain surfaces from PET images, it is favorable to approach the surface of interest from outside. The reason for this with PET brain surface extraction is that energy images usually contain more noise inside the brain volume than outside of it. For situations like this, we have developed a DSM-OS (DSM-outer surface) variant from our optimization algorithm. The DSM-OS algorithm uses only one surface mesh approaching the target from outside. The modification is straight-forward to implement. The energies of the outer mesh are recorded after each iteration and the energy of the outer mesh at the current iteration is compared to the lowest energy recorded. If the current energy is the lowest encountered so far, the mesh at that iteration is stored. The algorithm is stopped when the volume of the (outer) surface mesh becomes smaller than a given threshold and the mesh of the lowest energy (that was stored during the iteration of the algorithm) is returned as the extracted surface. For more details about the variant and advantages of it for brain surface extraction from PET images, see [6].

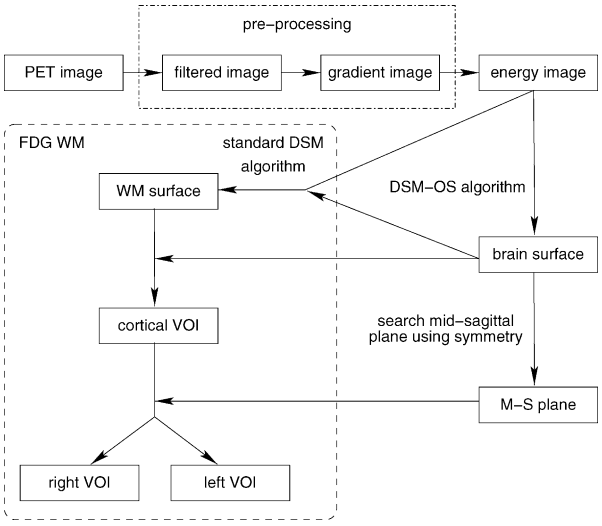

Fig. 2 Surface extraction and determination of volumes of interest (VOIs) automatically from PET brain images using the DM-DSM method and the mid-sagittal (M-S) plane. The white matter surface and cortical VOIs are only extracted from images from the FDG-PET studies.

4. Computational procedure for the DM-DSM method

In this section, we describe how the DM-DSM method has been implemented to extract the outer brain surface and the 'white matter' surface automatically from the PET brain images. Determination of the mid-sagittal plane is performed using the extracted brain surfaces. A flowchart of the procedure is presented in Fig. 2.

4.1. Computation of energy images

4.1.1. FDG-PET

As mentioned earlier, intensity values in an energy image should ideally be high at the voxels belonging to surface of interest and low elsewhere in the energy image. With the FDG, edges in the original images seem to be a good and simple feature characterizing surfaces of interest. We define the energy image for the FDG as

$$B_{\mathrm{FDG}} = \|\nabla \mathrm{MF}(I)\|, \tag{6}$$

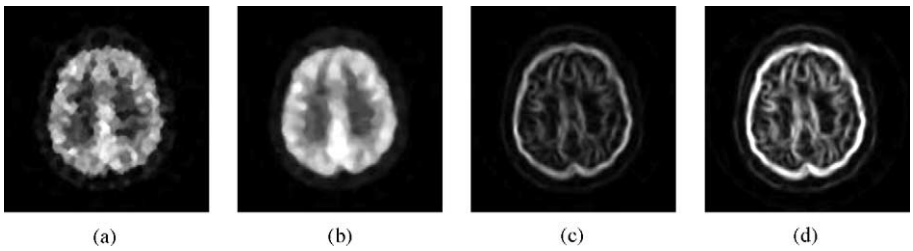

Fig. 3 Steps in energy image computation in the case of the FDG-PET brain images. Transaxial image cross-sections from (a) the original image, (b) the median filtered image, (c) the gradient image and (d) the energy image, which is a contrast enhanced version of the gradient image in (c).

where I is the FDG-PET image to processed and MF denotes a median filter. The gradient is computed by the 3D Sobel operator [29]. In practice, the energy image B_{FDG} can contain few aberrantly large intensity values, which reduce the contrast in other parts of the image. Therefore, to improve the contrast, a certain (small) percentage of largest intensity values receive intensity value 1 in the normalized version of the energy image. The steps for computing B_{FDG} are depicted in Fig. 3.

4.1.2. Raclopride PET

For brain surface extraction from Raclopride PET images, constructing energy images requires somewhat more effort than in the case of FDG-PET images. The whole process is depicted in Fig. 4.

The highest tracer uptake present in the images is within the striatum and tracer uptake elsewhere in the brain volume is rather low [30]. This can be seen also from Fig. 4(a). Therefore, energy images computed as with the FDG tracer would show higher intensity values at boundaries of the striatum than at the brain surface. As we would like most salient voxels to lie on the brain surface, we determine which voxels are likely to belong to the striatum after median filtering the Raclopride images. The determination is based on the expected volume of the striatum and the assumption that the striatum consists of voxels with the highest intensity values in the image. For an adult, the total volume of the striatum is about 20 cm^3 [31]. Intensity values within the so-determined striatum are then replaced by the average intensity value of the image, cf. Fig. 4(c). In this way, we do not need to concerned about voxels, which have been incorrectly classified as those belonging to the striatum and we can set the threshold for the volume of striatum to be larger than 20 cm^3. After this, we apply a gray-level morphological opening with a flat and symmetric structuring function to the image to reduce disturbances resulting from tracer distribution outside the brain volume [32].

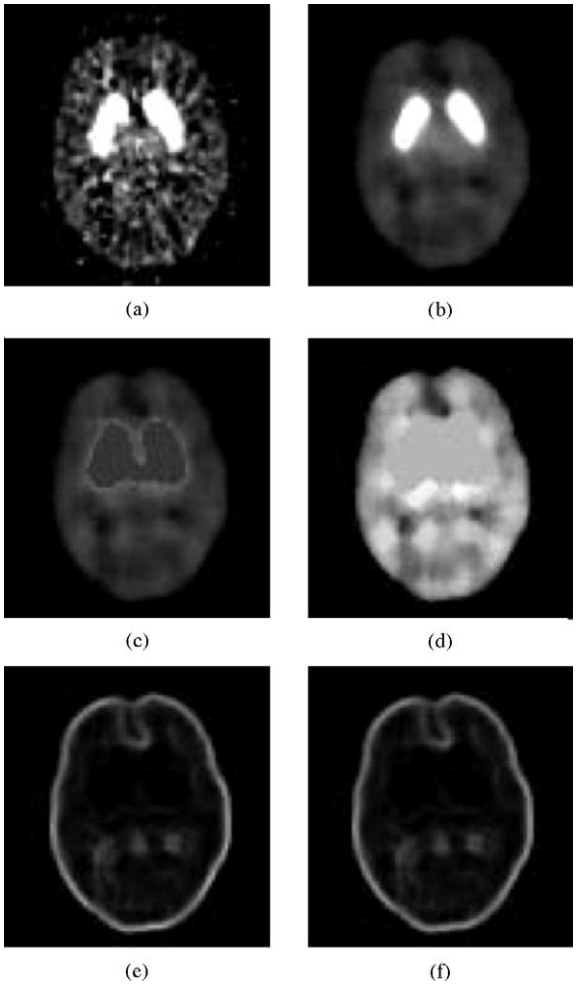

Fig. 4 Steps in energy image computation in the case of the ^{11}C-Raclopride brain images. Transaxial image cross-sections from (a) the original image, (b) the median filtered image, (c) the image where high intensity values in striatum have been replaced by the average intensity value of the image, (d) the image after morphological filtering, (e) the energy image before contrast enhancing normalization and (f) the energy image. In (a and b), highest intensity values (in striatum) have been scaled down in order to make low intensity values elsewhere in the brain volume visible.

After the pre-processing steps (Fig. 4(d)), voxels just outside the brain volume have low intensity values and voxels within the brain volume have at least moderate intensity values. Hence, for voxels just outside the brain volume the values of the gradient magnitude image are relatively high and we set

$$B_{\text{Raclopride}}(\boldsymbol{x}) = \|\nabla I_{\text{F}}(\boldsymbol{x})\|(1 - I_{\text{F}}(\boldsymbol{x})), \tag{7}$$

where $B_{\text{Raclopride}}$ is the energy image for the Raclopride PET images and I_{F} (as in Fig. 4(d)) denotes the pre-processed image. Intensity values of I_{F} are normalized to lie in the range $[0, 1]$ and the gradient is computed as with the FDG images. We improve the contrast of the energy images in the same way as with the FDG-PET images.

4.2. Delineation of the brain surface

In the energy image (Figs. 3(d) and 4(f)), the brain surface has relatively high contrast against background. Also, the noise level outside of the brain volume is considerably lower than inside of it in the energy image. Hence, we apply the DSM-OS modification approaching the brain surface from outside for extraction of it.

For automatic generation of the initialization for the deformable model, we assume that the centre point of the brain is located near the mass centre of voxel intensities in the original image. A large ellipsoid, as compared to the image dimensions, is used as the initial surface. The centre of the ellipsoid is set into the mass centre of voxel intensities. An example of this kind of initialization is shown in Fig. 5. From this, the DM-DSM method (using DSM-OS algorithm) delineates the surface of brain. The thin-plate shape model is used in the brain surface extraction.

4.3. Determination of the mid-sagittal plane

For extraction of the mid-sagittal plane, we applied an existing method originally designed for anatomical brain images [26]. Instead of edge images, we apply the extracted brain surfaces as the basis for mid-sagittal plane extraction. Hence, we define the mid-sagittal plane as the one about which the reflective symmetry of the brain surface is maximized.

The algorithm used in this study is highly similar to the one described in [26] and therefore we describe it here only briefly. The algorithm first determines the slope of the symmetry axis on each axial slice of the image. This is done by maximizing the cross-correlation between the brain contour on the current slice rotated by the angle θ and vertically reflected version of the brain contour rotated by the angle $-\theta$. Brain contours are intersections of the brain surface and axial image cross-sections. Thereafter, the slopes of the symmetry axes on each slice are combined to yield an estimate $\hat{\theta}$ of the common slope of the intersection of the mid-sagittal plane and transaxial cross-sections by using a robust estimation technique. Once we have obtained the estimate $\hat{\theta}$, offsets of the mid-sagittal plane to the symmetry axis defined by $\hat{\theta}$ on each slice can be computed again by maximizing the cross-correlation of the brain contours on each axial slice. Based on these offsets the robust least median of squares regression [33] is used to determine the remaining parameters required for specifying the mid-sagittal plane.

Fig. 5 Automatically generated initialization for the search of the brain surface shown on the PET image. From top, the sagittal, coronal and transaxial cross-section views.

4.4. Extraction of the white matter surface

We apply the standard DSM-algorithm for extraction of the white matter surface. The white matter surface is the boundary between the tracer uptake levels in the gray matter and white matter tissues that is visible in FDG-PET images. The delineated white matter surface together with the brain sur-

face defines the coarse cortical structure in the image. To avoid the deformable mesh from converging again to the brain surface, high intensity values relating to the brain surface are removed from the energy image. This is done based on the previously extracted brain surface. The already found brain surface can also be used for generating initializations for the DSM algorithm. The inner and outer initial surfaces are created from it by scaling. Both shape models, the thin-plate and the sphere, can be applied to the extraction of the white matter surface.

4.5. Hardware and software specifications

The DM-DSM method was implemented in MATLAB® (Version 5.3, Mathworks, Natick, MA, US). The surface extraction results for this study was calculated in the AlphaServer 4100 with 21164A (EV5.6) processors. The time for the whole process was approximately 20 min per image with the material used in this study. The automatic surface extraction step, the DSM algorithm, has now been implemented as an object-oriented C++ program. The dualsurfacemin software is freely available at http://www.cs.uta.fi/research/software/.

5. Materials for sample runs

Brain surface extraction and the determination of the mid-sagittal plane were evaluated with images from a phantom study and images from ^{18}FDG-PET and ^{11}C-Raclopride PET studies of healthy volunteers. The white matter surface was extracted from the phantom images and the FDG images. The Hoffman brain phantom (JB003, Nuclemed N.V./S.A., Roeselare, Belgium) was filled with ^{18}FDG. Structures corresponding to cerebellum, cortex, basal ganglia and ventricles are represented in the phantom.

All the PET acquisitions were made with the GE Advance scanner (GE, Milwaukee, USA). The FDG-PET images were reconstructed with the iterative MRP method to the cross-section image size of 128×128 [10]. The voxel size was $1.72\,\text{mm} \times 1.72\,\text{mm} \times 4.25\,\text{mm}$. The Raclopride PET images were reconstructed with the FBP method to the same image size than the FDG images. The voxel size was $2.3\,\text{mm} \times 2.3\,\text{mm} \times 4.25\,\text{mm}$.

From the phantom study, we created two images where the brain was in two different orientations, mainly to test the algorithm for determining the mid-sagittal plane. In the one image, the brain was in the neurological orientation and in the other it was slightly rotated from this orientation. The resulting images are called the original phantom and the rotated phantom, respectively. The rotation was implemented using the AIR software [34], and the rotation angles were 5° in the transaxial plane (yaw), 0° in the sagittal plane (pitch) and 3° in the coronal plane (roll). Rotations were performed in the order yaw, pitch and roll.

The pixel by pixel Patlak model [35] was applied to the FDG sinograms to produce parametric images to be used in the delineation process. The Raclopride images were calculated to parametric images showing the Raclopride binding with a simplified reference model [36].

The evaluated parameter ranges for the surface extraction method were based on our earlier experiments in [8]. Surface extraction was tested with the meshes of 320, 960 and 1280 mexels. The value of regularisation parameter λ was varied in the range 0–0.5 for the search. Extraction of the white matter surface, where we apply the standard DSM-algorithm, was performed with two types of initializations: initial surfaces were generated from an ellipsoid or from the extracted brain surface. These called, respectively, the ellipsoid initialization and the brain surface initialization. The thin-plate and the sphere prior shapes were tested for the white matter surface extraction. The evaluation was based on visual comparison of the extracted surface to the energy image and the original image, and in the case of FDG also to manually segmented reference. The parameter values from the phantom study were used for extraction of surfaces from the images of seventeen FDG and four Raclopride brain studies.

The brain volumes were segmented from the original FDG images for the quantitative assessment of the extracted brain surfaces by using an interactive thresholding method [3]. The threshold was visually adjusted for each individual FDG brain image in such a way that the brain volume could be accurately extracted from the image. Due to noise and inhomogeneities in the original image, the resulting volume needed further manual editing in all cases to end up with continuous volumes without holes or handles. These brain volumes were used as references for evaluation of the accuracy of the automatic method for extracting the brain surface. In a similar way, the gray matter volume was segmented from the image of the Hoffman phantom to be applied as a reference volume for evaluating the performance of our method in the determination of the white matter surface. The interactively segmented reference volumes were compared to the automatically extracted ones by using the Jaccard coefficient as the measure of similarity [37].

The extracted brain volumes were composed of the voxels inside of or intersected by the brain surface meshes. The Jaccard coefficient J_c is defined by

$$J_c = \frac{|A \cap B|}{|A \cup B|}, \tag{8}$$

where A is the set of voxels within the reference volume and B is the set of voxels within the extracted volume. The Jaccard coefficient is a frequently applied similarity measure when evaluating image segmentation results. The values of J_c are in the range from 0 to 1. The value zero means that A and B share no voxels and the value one means that A and B are equal.

We also computed the directed mean Hausdorff distance measure [38] between the automatically extracted brain surfaces (denoted by S) and the reference brain surfaces (denoted by R) determined as the set of boundary voxels of the reference brain volumes. An extracted surface S consists of the voxels that intersect with the surface mesh. We define the distance between the two to be

$$d(S, R) = \frac{1}{|R|} \sum_{r \in R} \min_{s \in S} \mathrm{dist}(s, r), \tag{9}$$

where $\mathrm{dist}(s, r)$ is the Euclidean distance between the centres of the voxels r and s. The Euclidean distance $\mathrm{dist}(s, r)$ can be computed in millimeters or as the distance between the integer coordinates of voxel centres. We refer to the latter as unit voxels. The distance $d(S, R)$ can be considered as the mean distance between digital surfaces S and R. Also other choices for the distance, such as the directed Hausdorff distance [38], would have been possible, but in our opinion the mean distance is more adequate here.

6. Results of sample runs

6.1. Phantom study

6.1.1. Brain surface

The accuracy of the extracted brain surfaces was excellent when the extracted surfaces were visually compared against the energy images as well as against the original images. The brain surfaces extracted from the rotated image and from the original image are shown in Fig. 6.

The initialization for the DSM-OS in the case of the original image was the one shown in Fig. 5. As can be seen from Fig. 6, there were no differences between visual qualities of the brain surface extracted from the original phantom image and the brain surface extracted from the rotated image.

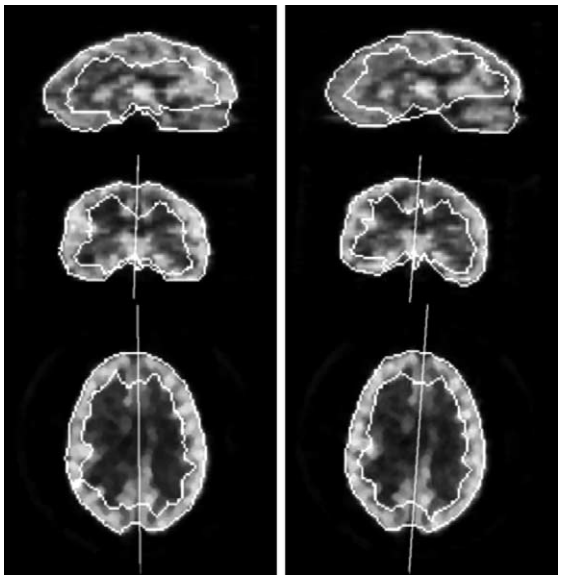

Fig. 6 The brain surface, white matter surface and mid-sagittal plane extracted from the original and the rotated Hoffman phantom image.

The extracted surfaces matched well with all surface details present in the energy images. The surface concavity at lower parts of the brain surface was also captured properly, as can be seen from the coronal cross-section in Fig. 6.

The results of the quantitative comparison against the interactively delineated reference brain volume were good. The J_c value was 0.906. The mean distance between the reference surface and the extracted surface was 1.237 mm (less than the shortest voxel side) and 0.518 in unit voxels.

The positioning of initial (ellipsoid) surfaces according to the mass centre of image intensities was found to be an appropriate method for initializing the DSM-OS algorithm. The DSM-OS algorithm was not sensitive to the size of the initial surface as long the surface of interest was located inside of it.

The number of mexels in a mesh should be sufficiently large for representing the surface to be extracted. The mesh size of 1280 mexels was found to be appropriate for the extraction of the brain surface. Details of the brain surface visible in images were properly captured with this mesh resolution. Meshes comprising 320 or 960 mexels could not accurately represent the brain surface.

In Eq. (1), the parameter λ defines relative weights of the internal energy and of the external energy. The brain surface was properly found with the evaluated range of values of parameter λ (0.05–0.5) and the DSM-OS algorithm was found to be rather insensitive to the value of λ in this case. We selected the value 0.3 from the evalu-

ated range for the use with the phantom images. However, also other choices would be possible, because the extracted surfaces with different values of λ were highly similar (differences in the J_c values were not significant). For the reasons explained in Section 4.2, the brain surface was extracted only using the thin-plate shape model.

6.1.2. Mid-sagittal plane

The mid-sagittal planes extracted from the original as well as the rotated phantom images were in a proper position and orientation when visually compared to the images. Intersections of the extracted mid-sagittal planes from the phantom images with transaxial and coronal image cross-sections are shown in Fig. 6.

The mid-sagittal plane extracted from the rotated phantom was rotated back with the inverse of the rotation applied for the generation of the rotated phantom. This way we could study the reproducibility of our method for delineation of the mid-sagittal plane. The dihedral angle between the two planes was 0.7°, the optimal dihedral angle would be 0°. The distances of the two planes from the image centre differed by 0.8 mm. The difference between the mid-sagittal plane from the original phantom and the 'back-rotated' mid-sagittal plane from the rotated phantom was negligible also when they were visually compared. The small difference can be mostly explained by the discrete nature of the algorithm for the mid-sagittal plane extraction.

6.1.3. White matter surface

The white matter surface was extracted with the ellipsoid and the brain surface initializations. The accuracy of delineated surfaces was comparable to the quality and the resolution of images with both initializations. However, with the ellipsoid initialization the DM-DSM method expressed sensitivity to the size of the inner initial surface mesh. Therefore, for automatic surface extraction, initializations generated based on the extracted brain surfaces would be the safer choice. The extracted white matter surfaces from phantom images with the brain surface initialization are shown in Fig. 6. With the brain surface initialization, the DM-DSM method was rather insensitive to the size of the search volume. The mesh size of 1280 mexels was found to be appropriate to capture the white matter surface from the phantom images. By using meshes of 320 or 960 mexels, the accuracy of the extracted surfaces was compromised by an insufficient mesh resolution. Both shape models, the thin-plate and the sphere, were examined for segmentation of the white matter surface. Extracted surfaces with the sphere shape model were slightly better in visual inspection.

The search process was more sensitive to the value of λ with the white matter surface than with the brain surface. Examples of the effect of the change of this value are shown in Fig. 7.

The sphere shape model was applied in these tests. If the shape regularisation was omitted ($\lambda = 0$), the DM-DSM method produced bumpy surfaces attracted by high intensity peaks in the energy image. An example is shown in Fig. 7(a), where the transaxial cross-section of the white matter surface seems to be of rather good quality, except for peaks of the surface visible near the middle of the image

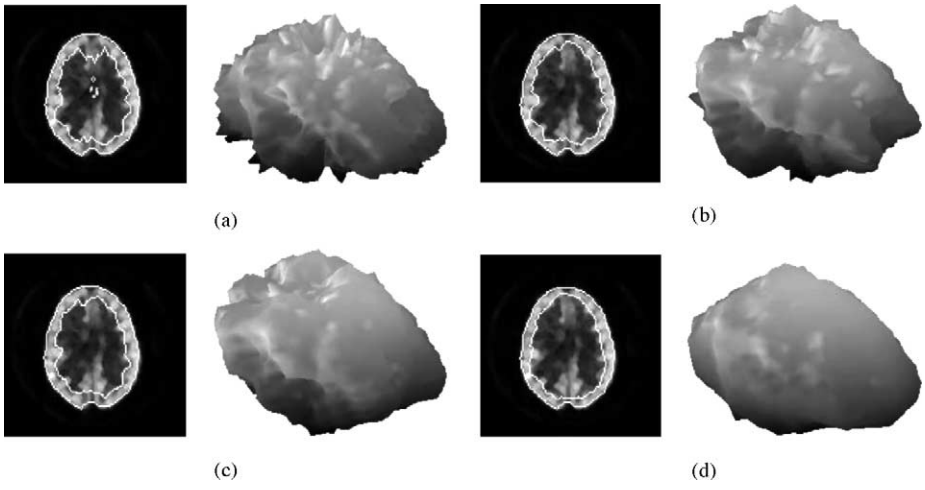

Fig. 7 The effect of the amount of the regularisation in searching of the white matter surface with the Hoffman phantom: (a) λ is zero, (b) $\lambda = 0.05$, (c) $\lambda = 0.2$ and (d) $\lambda = 0.5$. A transaxial cross-section is shown on the left column and a 3D rendering is shown on the right column. The smoothness of the mesh could not be controlled without the shape regularisation as shown in (a). The brain surface shown on the transaxial cross-sections is the same in all cases.

Table 1 Jaccard coefficients between the reference gray matter volume and the extracted gray matter volume from the phantom image

λ	J_c
0	0.456
0.05	0.492
0.2	0.494
0.5	0.322

Different values of λ were applied for extraction of the white matter surface

cross-section. The 3D rendering of the same surface in Fig. 7(a) better reveals that omitting shape regularisation compromises the smooth appearance of the resulting surface. Consequently, shape regularisation is needed for proper extraction of the surface. On the other hand, setting λ to 0.5 led to over-regularisation as can be seen from Fig. 7(d). Extracted white matter surfaces with values of λ set to 0.05 and 0.2 are depicted in Fig. 7(b) and (c). The white matter surfaces in Fig. 6 were both extracted with $\lambda = 0.2$.

Jaccard coefficient values between manually determined gray matter volumes and volumes extracted using the method proposed in this study are presented in Table 1.

The best value was obtained when the $\lambda = 0.2$ for the white matter extraction. The listed Jaccard coefficients are considerably lower than with the brain surface as expected. This is due the difficulty of the white matter surface extraction.

6.2. FDG and Raclopride brain studies

From the phantom tests, we obtained the parameter values for the evaluation of the DM-DSM method in the case of FDG and Raclopride brain studies. The mesh size of 1280 mexels was applied for all surfaces.

6.2.1. Brain surface

The brain surfaces delineated from all the 17 FDG-PET images were of excellent quality. In Fig. 8, examples of the cross-sections of the extracted brain surfaces from the FDG-PET images are overlayed on the corresponding energy images. In Fig. 9, same surface cross-sections divided to left and right hemispheres are overlayed on the original FDG-PET images. The magnifications (by 500%) of the transaxial cross-sections in Fig. 8 shows how the extracted brain surfaces follow the details visible in the energy images. In Fig. 10, the 3D renderings of the two extracted brain surfaces depicted in Fig. 9 are shown together with the determined mid-sagittal planes.

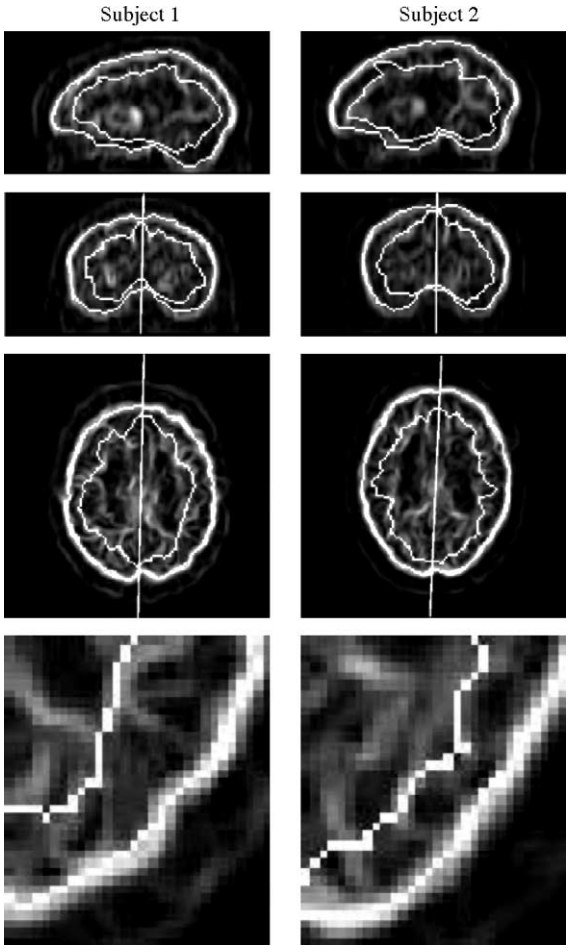

Fig. 8 Examples of the automatically delineated brain surfaces, mid-sagittal planes and white matter surfaces from the FDG-PET brain images of overlayed on the energy image. Based on the visual quality of the white matter surfaces, subject 1 is a typical result and subject 2 is the worst result, cf. the text. From top, the sagittal, coronal and transaxial cross-section views. The mid-sagittal plane is marked only on the coronal and the transaxial cross-sections. Bottom, magnifications (500%) of the lower right corner of the transaxial image cross-section are shown.

Jaccard coefficient values and distances between extracted and reference surfaces are presented in Table 2. The average (J_c) value was 0.909 which is similar to the one obtained with the phantom. In the worst case J_c was 0.841, which is clearly lower than the other values. The poorer quality of the extracted brain volume is probably due to the patient misalignment in the scanner, which has caused a part of the brain to be out of the field of view. The average distance between the extracted and reference surfaces was 1.618 mm and 0.647 unit voxels. These values are a bit higher than those obtained with the phan-

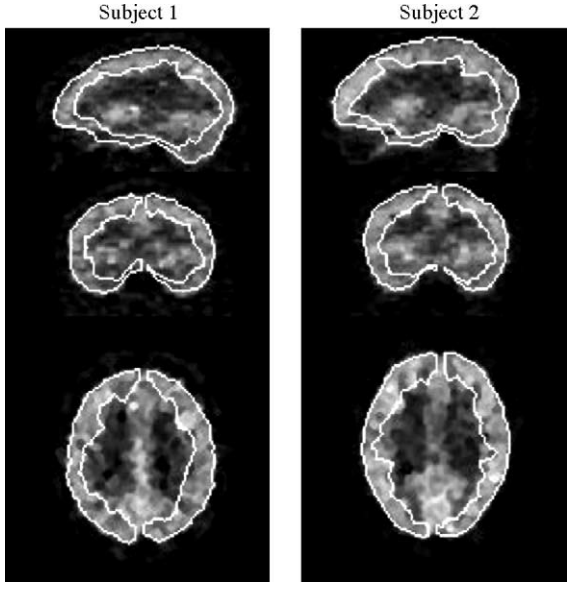

Fig. 9 The extracted VOIs overlayed on the original FDG-PET images.

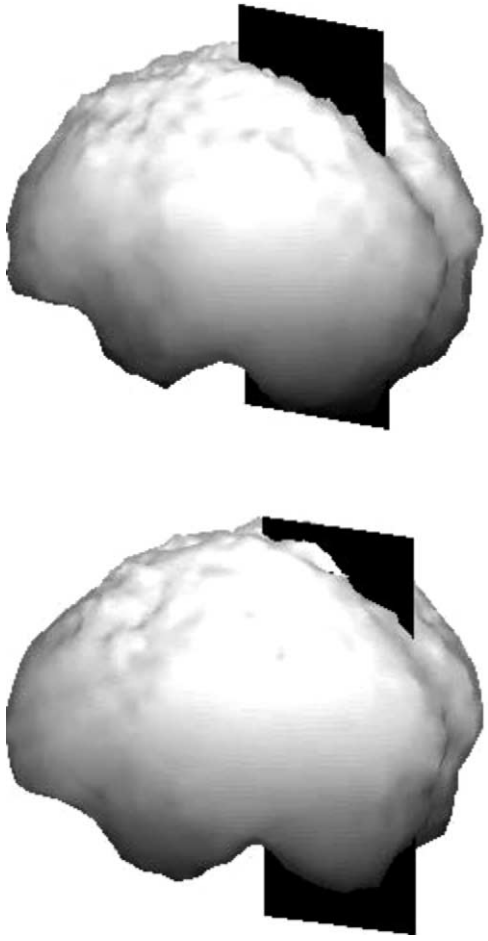

Fig. 10 Three-dimensional renderings of the brain surface meshes extracted from the FDG-PET brain images. The determined mid-sagittal planes are shown on black. From top, the subjects 1 and 2.

Table 2 The results from quantitative comparison between the automatically extracted the brain surfaces/volumes and the manually segmented (reference) brain surfaces/volumes from the 17 FDG-PET images and the phantom image

Study	J_c	Surface distance	
		voxels	mm
Phantom	0.906	0.518	1.237
1	0.910	0.706	1.810
2	0.928	0.506	1.218
3	0.934	0.421	0.965
4	0.926	0.513	1.267
5	0.924	0.484	1.154
6	0.898	0.669	1.757
7	0.900	0.802	2.139
8	0.884	1.004	2.609
9	0.915	0.523	1.208
10	0.916	0.565	1.378
11	0.912	0.583	1.439
12	0.912	0.655	1.664
13	0.903	0.724	1.880
14	0.917	0.542	1.289
15	0.923	0.521	1.272
16	0.841	1.148	2.947
17	0.910	0.629	1.515
Mean	0.909	0.647	1.618
S.D.	0.022	0.191	0.534

The column J_c refers to the Jaccard coefficients between the volumes. Two other columns list the distances between surfaces as in Eq. (9). The average values (mean) and standard deviation (S.D.) are computed from 17 FDG brain studies.

tom.

The visual quality of the brain surfaces extracted from the Raclopride images was nearly as good as with the FDG images. However, with the Raclopride PET images, the accuracy of the extracted brain surfaces was quite difficult to evaluate because brain volumes are barely visible in the original images. Fig. 11 presents one example of the extracted brain surface from Raclopride studies overlayed (a) on the original image and (b) on the energy image.

From the figure, it can be seen that the DM-DSM method was able to capture boundary concavity at lower parts of the brain remarkably well. In three cases out of the four studied, the delineated surfaces were of similar quality as the one depicted in Fig. 11. Only in a single case out of the four there were minor but clear errors in the delineated surface. These errors were explainable by imperfections in the energy image.

As with the phantom studies, positioning the initial (ellipsoid) surface according to the mass centre of intensity values in the images was found to be an

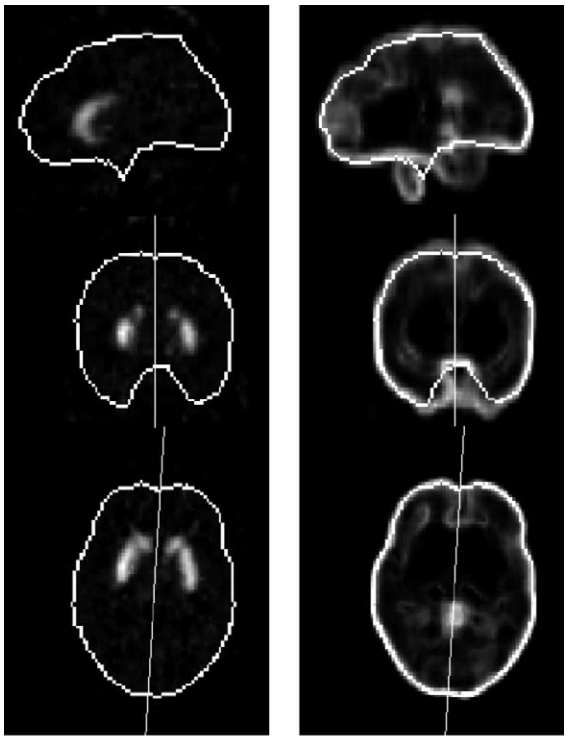

Fig. 11 Extracted brain surface and mid-sagittal plane from the Raclopride brain image overlayed on (a) the original image and (b) the energy image. From top, sagittal, coronal and transaxial cross-section views.

appropriate method to generate initializations for the DSM-OS algorithm. Due to individual variations in the size of the brain, practically the whole image volume needs to be inside the initial ellipsoid for automatic search. This did not present any problems for the DSM-OS algorithm, although initializations were quite far from the surfaces of interest. The thin-plate shape model was used for the search of the brain surface as with the phantom study. The effect of the value of the parameter λ was found to be minimal in extraction of the brain surface in the human studies. The same value ($\lambda = 0.3$) as with the phantom study was chosen. All the brain surfaces from the FDG-PET and the Raclopride PET images in Figs. 8–11 were extracted using this value of the parameter.

The steps required for generation of the energy images with the Raclopride tracer were different from those with the FDG tracer. The distinct uptake of this kind of receptor tracers concentrates almost only in striatum and the other areas of the brain image remain almost invisible and have a very low contrast to the background. In pre-processing, the removal of the striatum was needed for defining a proper energy image for the search of the brain surface. The volume of striatum was always overestimated. This did not cause any problem for the search, since the intensity values of the volume were replaced with the average intensity value of the image. Except that the external energy function was different, we could apply exactly the same processing steps for all the four Raclopride images without user interaction.

6.2.2. Mid-sagittal plane

The mid-sagittal plane was automatically determined based on the extracted brain surfaces for all the 17 FDG-PET and the 4 Raclopride PET images. The extracted mid-sagittal planes are depicted on transaxial and coronal cross-sections in Figs. 8, 9 and 11. The position and orientation of the mid-sagittal plane was proper in visual inspection of every image. Especially, minor errors in the extracted brain surface from one of the Raclopride images did not compromise the robustness of mid-sagittal plane determination.

6.2.3. White matter surface from FDG images

For the white matter surface, the found brain surface was used for generating the initial surfaces for the standard DSM algorithm. Because the noise level in the FDG brain images was significantly higher than in the phantom image, we tested white matter surface extraction with different values of the parameter λ also in this case. The best value of λ was found to be 0.2 (tested range 0.05–0.4). The applicable range for value of λ was narrower than with the phantom study.

The visual quality of delineated surfaces varied more with the white matter surface than with the brain surface. The example images shown in Figs. 8 and 9 were chosen and ranked based on the visual quality of the extracted white matter surfaces. The result of subject 1 represents typical quality of the delineated white matter surface. In the worst case, subject 2, the extracted surface had a clear spike diverging from 'the correct' white matter surface. This spike can be seen on top of the sagittal cross-section view in Fig. 8. However, there were no clear differences in the visual quality of the delineated surfaces when they were compared to the energy images, see the magnifications in Fig. 8. The difference in goodness between the best and typical surfaces was quite marginal and the ranking is therefore highly subjective. The division of the cortical VOIs into left and right hemispheres based on the mid-sagittal planes is depicted in Fig. 9.

6.3. Quantitative evaluation with simulated data

We have evaluated quantitatively the DM-DSM method for the automatic brain surface extraction from PET images with the Monte Carlo simulated data in [39]. We briefly summarize the evaluation here.

For the tests, we generated realistic dynamic PET images for the FDG and Raclopride radiopharmaceuticals using the PET SORTEO software [40]. An energy image for the deformable model was calculated from a time-averaged PET image. The parametric image was additionally applied to create the energy image with the case of Raclopride. The pose and position of the brain structure, and the regularisation parameter λ were varied to test sensitivity of the surface extraction method. The mean Jaccard coefficient values between automatically extracted brain volumes and the reference brain volumes were from 0.893 to 0.940 for the FDG and from 0.769 to 0.842 for the the Raclopride images. The deformable model was insensitive to the value of the regularisation parameter. The DM-DSM method allowed for accurate extraction of the brain surfaces regardless of the pose or position of the brain in the image.

6.4. Summary of results

The brain surfaces were automatically extracted from two completely different types of PET images: the FDG-PET images and the Raclopride PET images. All the brain surfaces were accurate in visual inspection as compared to the image resolution. Also, boundary concavities within lower parts of the brain surfaces were captured properly. The computed quantitative measures of the brain surface quality were in line with the conclusions of the visual inspection. Determination of the mid-sagittal plane was automatic for all the images. This task could be challenging for Raclopride images if only image intensity values were to be used for it. By combining the brain surface, the mid-sagittal plane and the white matter surface, we were able to determine the left cortical and the right cortical VOIs from the PET-FDG images without user interactions, see the transaxial and the coronal cross-sections in Fig. 9.

7. Discussion and future plans

We have applied a deformable model based DM-DSM method for the demanding surface extraction problems arising with functional positron emission tomography brain images. In this study, we demonstrated that the brain surfaces from both the FDG and Raclopride images could be automatically delineated with the new global optimization-based deformable model. The surface extraction procedure and the parameters for the deformable model were the same with both radiopharmaceuticals, only the definitions of the energy images differed. The extracted brain surfaces were found to follow quite accurately the brain surfaces when compared to the original PET images as well as to the corresponding energy images. The brain surface provided a good basis for searching other surfaces from the brain images. We applied the delineated brain surfaces for the determination of the mid-sagittal plane of the brain. Together with the brain surface visualization, the mid-sagittal plane helps in orientation in the 3D brain image set for image registration purposes or for determination of volumes of interest. The extracted brain surface and white matter surface from the FDG images made it possible to determine the cortical VOIs automatically from the FDG images. With the found mid-sagittal planes these VOIs can be divided in two parts representing the two hemispheres. Although this may not be the sufficient way to delineate the gray matter volume from FDG-PET brain images, where the tracer uptake is highest in cortex, it shows that even with this kind of limited image quality there are possibilities to apply automatic means for surface extraction and determination of VOI.

Quantitative comparison between manually segmented reference surfaces and the extracted surfaces yielded good results, the mean value of the Jaccard coefficients was 0.909 with the images from FDG studies. Shattuck et al. [41] obtained the average $J_c = 0.910$ when evaluating their method for brain volume extraction (termed skull-stripping) from anatomical MR images with the Internet Brain Segmentation Repository (IBSR) dataset. We calculated also the mean distance from the points on the (digital) reference surface to the extracted (digital) surface. The average distance was 1.618 mm, which is less than the length of the shortest voxel side in the images. The quantitative evaluation with the simulated PET data, created by using the PET SORTEO software, further assured that the DM-DSM method allows for accurate extraction of brain surfaces [39,40].

Deformable surface models are methods that can extract geometrically continuous structures from noisy volumetric images. Surface extraction with them is formulated as an energy minimization problem allowing the incorporation of geometric prior information about the surface to be extracted.

However, as the energy function to be minimized usually has several local minima, its minimization is a challenging task. Particularly, the surface extraction result often depends highly on the initialization for the process limiting the automatic application of deformable models. In this study, we have minimized the energy of the deformable model either with the DSM algorithm or the DSM-OS algorithm. For extraction of the brain surface where it is favorable to approach the surface of interest from outside, we applied the DSM-OS algorithm capable of taking advantage of such prior knowledge. The standard DSM algorithm was applied for extraction of the white matter surface, where it is hard to specify the best direction to approach the surface of interest. These algorithms are global in the sense that they are able to overcome local minima. Hence, the problems with initialization sensitivity are considerably reduced with these algorithms, even if they feature some sensitivity to their initializations. This allowed us to generate initial surfaces for the algorithms automatically without any references to anatomical images. For this reason extracted surfaces can be applied for registration purposes with the surface-based methods. The applied optimization algorithms are also deterministic, which is important for reproducibility of the results. Another important merit of the applied deformable model for this study was that it could be applied to brain surface extraction both from the Raclopride and FDG-PET images. Moreover, the model parameters and the initialization process were the same in both cases, which is of importance for automatic surface extraction. Distinguishable features in a PET image depend highly on the applied radiopharmaceutical. However, the tracer distribution in the images has always some correspondence to anatomical structures, and because the tracer circulates in the blood also structures like the whole brain can be detected with all the tracers. The edge-detection method used with the FDG images, i.e using image gradients as features of interest, would not lead to good results for brain surface extraction from the Raclopride images. Designing suitable energy images for them required somewhat more effort. Nevertheless, the computation of energy images for the Raclopride tracer was still quite simple and it did not require assumptions, e.g. about the parametric form of the probability density function of image histograms.

The identification of the brain surface and separation of hemispheres are starting points for extraction of other surfaces and structures from the brain image. In this study, we extracted the white matter surface with the DM-DSM method from the FDG images after delineation of the brain surface. In a similar way, also other structures visible in the images could iteratively be extracted by starting from, for example, regions of the highest uptake of the radiopharmaceutical, or from the largest structures. We have presented the principal idea of this kind of analysis with the preliminary results in [7]. Then, we have applied this idea to automatically identify the striatum structure from the PET images for improving reproducibility in the dopamine D_2-receptor studies [42]. In addition, the noisy PET images are difficult to compress by using lossless methods [43,44]. The extracted brain structure information could be applied to improve lossless compression of PET brain images.

Acknowledgements

The authors would like to thank the Turku PET Centre for providing PET images for evaluation. This study was financially supported by Tampere Graduate School in Information Science and Engineering (TISE), the Academy of Finland and Tekes (Drug2000 Technology Program).

References

[1] R.H. Huesman, G.J. Klein, B.W. Reutter, X. Teng, Multiscale PET quantitation using three-dimensional volumes of interest, in: R.E. Carson, P. Herscovitch, M. Daude-Witherspoon (Eds.), Quantitative Functional Brain Imaging with Positron Emission Tomography, Academic Press, 1998, pp. 51—58 (Chapter 8).

[2] B.F. Hutton, M. Braun, L. Thurfjell, D.Y.H. Lau, Image registration: an essential tool for nuclear medicine, Eur. J. Nucl. Med. 29 (January (4)) (2002) 559—577.

[3] J. Mykkänen, M. Juhola, U. Ruotsalainen, Extracting VOIs from brain PET images, Int. J. Med. Inform. 58–59 (2000) 51—57.

[4] K.F. Lai, R.T. Chin, Deformable contours – modelling and extraction, IEEE Trans. Pattern Anal. Machine Intell. 17 (11) (1995) 1084—1090.

[5] J. Mykkänen, J. Tohka, U. Ruotsalainen, Automated delineation of brain structures with snakes in PET, in: A. Gjedde, S.B. Hansen, G.M. Knudsen, O.B. Paulson (Eds.), Physiological Imaging of the Brain with PET, Academic Press, 2001, pp. 39—43.

[6] J. Tohka, J.M. Mykkänen, Deformable mesh for automated surface extraction from noisy images, Int. J. Image Graph. 4 (2004) 405—432.

[7] U. Ruotsalainen, J. Mykkänen, J. Luoma, J. Tohka, S. Alenius, Methods to improve repeatability in quantification of brain PET images, in: F. Rattay (Eds.), World Congress on Neuroinformatics, ARGESIM Report 20, ARGESIM/ASIM Verlag, Vienna 2001, pp. 659—664.

[8] J. Mykkänen, J. Tohka, U. Ruotsalainen, Delineation of brain structures from positron emission tomography images using deformable models, in: R. Baud, M. Fieschi, P. Le Beaux, P. Ruch (Eds.), The New Navigators: From Professionals to Patients, Stud. Health. Technol. Inform., vol. 95, IOS Press, 2003, pp. 33—38.

[9] J. Luoma, Extracting hemisphere structures automatically from brain PET images, in: J., Knuuti, K., Någren (Eds.), Abstracts of the IX Turku PET Symposium, number D 499 in Annales Universitatis Turkuensis, University of Turku, May 25—28, 2002, p. Q4.
[10] S. Alenius, U. Ruotsalainen, Generalization of median root prior reconstruction, IEEE Trans. Med. Imaging 21 (11) (2002) 1413—1420.
[11] T. McInerney, D. Terzopoulos, Deformable models in medical image analysis: a survey, Med. Image Anal. 1 (2) (1996) 91—108.
[12] D. MacDonald, N. Kabani, D. Avis, A.C. Evans, Automated 3-D extraction of inner and outer surfaces of cerebral cortex from MRI, NeuroImage 12 (3) (2000) 340—358.
[13] C. Xu, D.L. Pham, M.E. Rettmann, D.N. Yu, J.L. Prince, Reconstruction of the human cerebral cortex from magnetic resonance images, IEEE Trans. Med. Imaging 18 (6) (1999) 467—479.
[14] C. Xu, J.L. Prince, Generalized gradient vector flow external forces for active contours, Signal Process. 71 (2) (1998) 131—139.
[15] D. Shen, E.H. Herskovits, C. Davatzikos, An adaptive focus statistical shape model for segmentation and shape modeling of 3D brain structures, IEEE Trans. Med. Imaging 20 (April(4)) (2001) 257—270.
[16] E. Bardinet, L.D. Cohen, N. Ayache, A parametric deformble model to fit unstuctured 3D data, Comput. Vis. Image Understand. 71 (July(1)) (1998) 39—54.
[17] R. Noumeir, R. El-Daccache, Attenuation correction in SPECT using active surfaces, Proc. IEEE Nucl. Sci. Symp. 3 (1998), pp. 1995—1999.
[18] L.D. Cohen, I. Cohen, Finite-element method for active contour models and balloons for 2-D and 3-D images, IEEE Trans. Pattern Anal. Machine Intell. 15 (November(11)) (1993) 1131—1147.
[19] M. Kass, A. Witkin, D. Terzopoulos, Snakes: Active contour models, Int. J. Comput. Vis. 1 (1987) 321—331.
[20] G.J. Klein, R.H. Huesman, Four-dimensional processing of deformable cardiac PET data, Med. Image Anal. 6 (1) (2002) 29—46.
[21] E. Debreuve, G. Aubert, M. Barlaud, I. Laurette, J. Darcourt, Space-time segementation using level set active contours applied to myocardial gated SPECT, IEEE Trans. Med. Imaging 20 (7) (2001) 643—659.
[22] R. Malladi, J. Sethian, B.C. Vemuri, Shape modelling with front progagation: a level set approach, IEEE Trans. Pattern Anal. Machine Intell. 17 (February(2)) (1995) 158—175.
[23] J. Tohka, Surface extraction from volumetric images using deformable meshes: a comparative study, Proceedings of seventh European Conference on Computer Vision, no. 2352, Lect. Notes Comput. Sci. (2002) 350—364.
[24] B.A. Ardekani, J. Kershaw, M. Braun, I. Kanno, Automatic detection of the mid-sagittal plane in 3-D brain images, IEEE Trans. Med. Imaging 16 (12) (1997) 947—954.
[25] S. Prima, S. Oursein, N. Ayache, Computation of the mid-sagittal plane in 3-D brain images, IEEE Trans. Med. Imaging 21 (2) (2002) 122—138.
[26] Y. Liu, R.T. Collins, W.E. Rothfus, Robust midsagittal plane extraction from normal and pathological 3-D neuroradiology images, IEEE Trans. Med. Imaging 20 (3) (2001) 175—192.
[27] H. Delingette, General object reconstruction based on simplex meshes, Int. J. Comput. Vis. 32 (1999) 111—142.
[28] D.J. Williams, M. Shah, A fast algorithm for active contours and curvature estimation, CVGIP: Image Understand. 55 (1) (1992) 14—26.
[29] S. Zucker, R. Hummel, A three-dimensional edge operator, IEEE Trans. Pattern Anal. Machine Intell. 3 (3) (1981) 324—331.
[30] J. Hietala, K. Någren, P. Lehikoinen, U. Ruotsalainen, E. Syvälahti, Measurement of striatal D_2 dopamine receptor density and affinity with ^{11}C-Raclopride in vivo: a test-retest analysis, J. Cereb. Blood Flow Metabol. 19 (2) (1999) 210—217.
[31] G. Firnau, E.S. Garnett, R. Chirakal, S. Sood, C. Nahmias, G. Schrobilgen, [^{18}F]fluoro-L-dopa for the in vivo study of intracerebral dopamine, Appl. Radiat. Isot. 37 (8) (1986) 669—675.
[32] H.J.A.M. Heijmans, Theoretical aspects of gray-level morphology, IEEE Trans. Pattern Anal. Machine Intell. 13 (June(6)) (1991) 568—582.
[33] P.J. Rousseeuw, A.M. Leroy, Robust Regression and Outlier Detection, Wiley-Interscience, New York, 1987.
[34] R.P. Woods, J.C. Mazziotta, S.R. Cherry, MRI-PET registration with automated algorithm, J. Comput. Assist. Tomogr. 17 (4) (1993) 536—546.
[35] C.S. Patlak, R.G. Blasberg, Graphical evaluation of blood-to-brain transfer constants from multiple uptake data. Generalizations, J. Cereb. Blood Flow Metabol. 5 (1985) 584—590.
[36] R.N. Gunn, A.A. Lammertsma, S.P. Hume, V.J. Cunningham, Parametric imaging of ligand-receptor binding in PET using a simplified reference region model, NeuroImage 6 (1997) 279—287.
[37] D.A. Jackson, K.M. Somers, H.H. Harvey, Similarity coefficients: measures of co-occurrence and association or simply measures of occurrence? Am. Nat. 133 (3) (1989) 436—453.
[38] J.S.M. Vergeest, S. Spanjaard, Y. Song, Directed mean Hausdorff distance of parameterized freeform shapes in 3D: a case study, Vis. Comput. 19 (2003) 480—492.
[39] J. Tohka, A. Kivimäki, A. Reilhac, J. Mykkänen, U. Ruotsalainen, Assessment of brain surface extraction from PET images using Monte Carlo simulations, IEEE Trans. Nucl. Sci. 51 (5) (2004) 2641—2648.
[40] A. Reilhac, C. Lartizien, N. Costes, S. Sans, C. Comtat, R.N. Gunn, A.C. Evans, PET-SORTEO: A Monte Carlo-based simulator with high count rate capabilities, IEEE Trans. Nucl. Sci. 51 (2004) 46—52.
[41] D.W. Shattuck, S.R. Sandor-Leahy, K.A. Schaper, D.A. Rottenberg, R.M. Leahy, Magnetic resonance image tissue classification using a partial volume model, NeuroImage 13 (5) (2001) 856—876.
[42] J. Tohka, E. Wallius, J. Hirvonen, J. Hietala, U. Ruotsalainen, Improved reproducibility in dopamine D_2-receptor studies with automatic segmentation of striatum from PET images, Proceedings of IEEE Medical Imaging Conference (MIC2004), 2004.
[43] J. Mykkänen, T. Tossavainen, M. Juhola, Lossless compression of emission tomography images, in: A. Hasman, B. Blobel, J. Dudeck, R. Engelbrecht, G. Gell, H.-U. Prokosch (Eds.), Medical Infobahn for Europe, Proceedings of MIE2000 and GMDS2000, Stud. Health. Technol. Inform., vol. 77, IOS Press, 2000, pp. 1240—1244.
[44] J. Mykkänen, Lossless compression of FDG-PET brain images: first experiments with JPEG, 1st Nordic Workshop on Brain Imaging and Neuroinformatics, Tampere University of Technology, 2003.